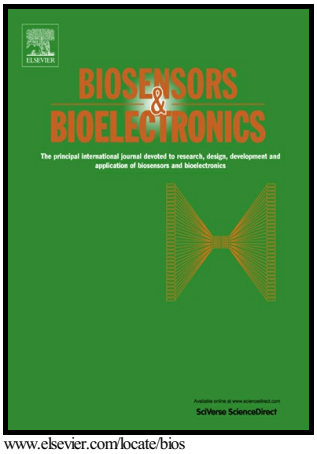

www.elsevier.com/locate/bios

Facile one-pot synthesis of visible light-responsive $BiPO_4$/nitrogen doped graphene hydrogel for fabricating label-free photoelectrochemical tetracycline aptasensor

Lan Ge, Henan Li, Xiaojiao Du, Mingyue Zhu, Wei Chen, Tingyan Shi, Nan Hao, Qian Liu, Kun Wang

PII: S0956-5663(18)30270-7
DOI: https://doi.org/10.1016/j.bios.2018.04.008
Reference: BIOS10404

To appear in: *Biosensors and Bioelectronic*

Received date: 1 February 2018
Revised date: 29 March 2018
Accepted date: 6 April 2018

Cite this article as: Lan Ge, Henan Li, Xiaojiao Du, Mingyue Zhu, Wei Chen, Tingyan Shi, Nan Hao, Qian Liu and Kun Wang, Facile one-pot synthesis of visible light-responsive $BiPO_4$/nitrogen doped graphene hydrogel for fabricating label-free photoelectrochemical tetracycline aptasensor, *Biosensors and Bioelectronic,* https://doi.org/10.1016/j.bios.2018.04.008

Facile one-pot synthesis of visible light-responsive $BiPO_4$/nitrogen doped graphene hydrogel for fabricating label-free photoelectrochemical tetracycline aptasensor

Lan Ge[a], Henan Li[a], Xiaojiao Du[a], Mingyue Zhu[a], Wei Chen[a], Tingyan Shi[a], Nan Hao[a], Qian Liu[a*] and Kun Wang[a,b*]

[a]Key Laboratory of Modern Agriculture Equipment and Technology, School of Chemistry and Chemical Engineering, Jiangsu University, Zhenjiang 212013, PR China

[b]Key Laboratory of Sensor Analysis of Tumor Marker, Ministry of Education, College of Chemistry and Molecular Engineering, Qingdao University of Science and Technology, Qingdao 266042, PR China

liuqian@ujs.edu.cn

wangkun@ujs.edu.cn

Abstract

It is fundamental to develop highly efficient visible light-responsive photoelectrochemical (PEC) performance material for fabricating PEC biosensor. Herein, $BiPO_4$/three-dimensional nitrogen doped graphene hydrogel (3DNGH) nanocomposites were prepared for the first time via a facile one-pot hydrothermal route. In this nanoarchitecture, the $BiPO_4$ nanorods were anchored onto the porous structure of 3DNGH. Compared with pristine $BiPO_4$, the absorption of $BiPO_4$/3DNGH has been extend to visible-light region, and the energy band gap of $BiPO_4$/3DNGH was calculated to be 2.10 eV, which was greatly narrower than that of pristine $BiPO_4$ with a band gap of 3.85 eV. Under visible light irradiation, the

photocurrent signal of the as-prepared $BiPO_4$/3DNGH was 847.2-fold, 4.1-fold and 2.3-fold enhanced comparing to pristine $BiPO_4$, $BiPO_4$ functionalized reduced graphene oxide and $BiPO_4$/nitrogen doped graphene. The enhancement of such photocurrent signal was attributed to the introduction of 3DNGH, which was capable to improve the charge transfer rate and also the efficiency of visible-light utilization of $BiPO_4$. Based on the excellent PEC properties of $BiPO_4$/3DNGH, a label-free PEC aptasensor for selectivity and sensitivity detection of tetracycline (Tc) was successfully established by using Tc aptamer as a biorecognition element. Under optimized conditions, the proposed PEC aptasensor exhibited a wide linear in the range from 0.1 nmol L^{-1} to 1 μmol L^{-1} as well as a low detection limit of 0.033 nmol L^{-1} (*S/N*=3). The prepared $BiPO_4$/3DNGH nanocomposites would serve as a promising visible light-responsive photoactive material for fabrication of PEC biosensors with high performance.

Keywords

Tetracycline; Nitrogen doped graphene hydrogel; $BiPO_4$ nanorod; Photoelectrochemical; Aptasensor

1. Introduction

Tetracycline (Tc) is one of a broad spectrum of antibiotics (Shen et al. 2014) against both Gram-negative and Gram-positive microorganisms, which were extensively used in human and veterinary treatment as well as feed additives due to its low cost and high antimicrobial activity (Gan et al. 2014). Excessive use of Tc in agriculture inevitably leads to their accumulation in diary food products such as milk, and eggs. Residues of Tc in food products may result in a risk to human health (Xu et

al. 2016a). European union (EU) has set the maximum residue limits (MRLs) for Tc as 0.3 mg kg^{-1} in liver, 0.6 mg kg^{-1} in kidney, 0.2 mg kg^{-1} in egg, and 0.1 mg kg^{-1} (about 200 nmol L^{-1}) in milk or muscle tissues (Hou et al. 2015). In China, the MRL for Tc was set at 0.05 mg/kg (about 100 nmol L^{-1}) (GB 21317—2007). Currently, various analytical methods for Tc detection have been developed, including high performance liquid chromatography (HPLC) (Liu et al. 2013) , liquid chromatography−mass spectrometry (LC-MS) (Bousova et al. 2013), colorimetric analysis (Hou et al. 2015; Ramezani et al. 2015), capillary electrophoresis (CE) (Ibarra et al. 2011) , fluorescence (Tan et al. 2013), chemiluminescence (Lau et al. 2004). Though, the aforementioned classical methods can provide precise and sensitive detection of Tc, these methods usually required complex operation, expensive equipment, or time-consuming operation procedures. Therefore, it is urgently needed to develop a rapid, simple, low-cost and specific method for the effective detection of Tc.

The photoelectrochemical (PEC) sensors based on the separation of the electrochemical signal and the light source have many advantages such as simple instrumentation setup, low cost, short analytical time, low background signal, and high sensitivity (Li et al. 2016; Zang et al. 2017). Typically, a general PEC biosensor necessitates two essential ingredients: the light source, and the PEC active species which convert light-irradiation to electrical signal. In a PEC biosensor, the intensity of the light source directly determines the electrical signal of the biosensor (Wang et al. 2016). However, the UV light, which only accounts for 2-4% of solar energy, is a high-energy excitation light source that easily resulting in fatal damage toward biomolecules (Chen et al. 2017a). Therefore, it is important to develop visible light-responsive photoactive material in PEC biosensors. Additionally, the

photoactive semiconductors (such as CdS quantum dots and TiO_2) with effective photoelectric conversion efficiency and superior biocompatibility were needed for the designing of PEC biosensors (Zhuang et al. 2015). However, the CdS QDs with certain toxicity could potentially damage biomolecules (Liu et al. 2016), which limited its practical applications. Bismuth phosphate ($BiPO_4$), as a novel non-poisonous photoactive material with ideal photoactivity, displayed a better photocatalytic performance than that of P25 (TiO_2) (Pan and Zhu 2010), which exhibited its potential applications in the fabrication of PEC biosensors. Nevertheless, a typical wide band gap (3.85 eV) of $BiPO_4$ makes them responsive only under UV irradiation that could potentially damage biomolecules. In order to improve the visible-light utilization efficiency of $BiPO_4$, several strategies have been devoted to combine $BiPO_4$ with other materials such as semiconductor (Lu et al. 2015), metal (Ye et al. 2015) and carbon-based materials (Tan et al. 2017) to form $BiPO_4$-based nanocomposites. Among them, the combination of graphene and $BiPO_4$ is an important method to improve the photoactive of $BiPO_4$. In our previous work, the fabricated $BiPO_4$ functionalized reduced graphene oxide ($BiPO_4$/rGO) nanocomposites revealed that graphene have an important role in promoting separating electron and hole pairs, leading to a high photocurrent (Qian et al. 2015). Therefore, the development of graphene-based nanocomposites is an effective method to improve the visible light activity performance of $BiPO_4$. With the deepening of the research, carbon nanomaterials doping heteroatoms have been developed into a research direction owing to its can effectively adjust their intrinsic properties (Liu et al. 2015b). Further studies showed that the differences of N (3.04) and C (2.55) electronegativity can create a unique electronic structure with the synergistic coupling effect between heteroatom dopants ,which can own much more active sites than most

singly doped carbonaceous materials (Mo et al. 2014). Therefore, nitrogen doped graphene is becoming one of prevailing photocatalysis, energy storage and environmental treatment (Wang et al. 2012). The recent emergence of three-dimensional nitrogen doped graphene hydrogel (3DNGH) has attracted great attention. Compared with two-dimensional nitrogen doped graphene (2DNG), 3DNGH not only possesses the intrinsic properties of graphene sheet but also owns exceptionally large accessible surface to increase active sites for immobilizing nanomaterials (Hao et al. 2017). Especially because of highly compressive strength, excellent electrical conductivity, and extremely large surface area, 3DNGH has become a promising candidate for electrochemical application such as energy storage (Choi et al. 2012) and conversion (Chen et al. 2011), biological and chemical sensing (Dong et al. 2012; Xi et al. 2013). Thus, it is meaningful to explore that the coupling of $BiPO_4$ and 3DNGH might have high performance in PEC sensor.

Herein, $BiPO_4$/3DNGH nanocomposites with excellent visible light-response were prepared by a one-pot hydrothermal route for the first time. The introduction of 3DNGH can efficiently improve the visible light absorption of $BiPO_4$, the energy band gap of $BiPO_4$/3DNGH to be 2.1 eV was greatly narrowed comparing to pristine $BiPO_4$ with a band gap of 3.85 eV, the fabricating $BiPO_4$/3DNGH nanocomposites possessed excellent PEC activity comparing to pristine $BiPO_4$, $BiPO_4$/rGO and $BiPO_4$/nitrogen doped graphene ($BiPO_4$/NG). On the basis of superior PEC performance of $BiPO_4$/3DNGH nanocomposites and label-free aptamer as a biorecognition element, a label-free sensing platform was successfully constructed. Furthermore, the PEC aptasensor based on $BiPO_4$/3DNGH nanocomposites was applied for sensitive and selective detection of Tc which was suitable for milk samples to confirm practical utility, indicating that $BiPO_4$/3DNGH nanocomposites

would be a promising visible light-responsive photoactive material for PEC biosensors.

2. Experimental section

2.1 Reagents and chemicals

$Bi(NO_3)_3 \cdot 5H_2O$, monosodium phosphate ($NaH_2PO_4 \cdot 2H_2O$), glycine and N,N-dimethylformamide (DMF) were purchased from Sinopharm Chemical Reagent Co., Ltd. Graphene oxide powder was purchased from Nanjing Xianfeng Nano Materials Technology Co., Ltd. The designed aptamer for Tc with the following sequence: 5′–CGTAC GGAAT TCGCT AGCCC CCCGG CAGGC CACGG CTTGG GTTGG TCCCA CTGCG CGTGG ATCCG AGCTC CACGT G–3′ was purchased from Sangon Biotech Co., Ltd. 0.1 mol L^{-1} phosphate buffered saline (PBS, pH 7.4) was used as the supporting electrolyte, which was prepared by mixing stock standard solutions of NaH_2PO_4 and Na_2HPO_4. All of the other chemical reagents used in our experiments were of analytical grade, and used without further purification. Ultrapure water was used throughout the study.

2.2 Apparatus

The scanning electron microscopy (SEM) were conducted on a field-emission scanning electron microscope (JSM-7001F Japan) equipped with an energy-dispersive spectroscopy (EDS, Oxford Inca Energy 400, UK). Transmission electron microscope (TEM) were performed by using a JEOL JSM-6700 transmission electron microscope. X-ray diffraction (XRD) patterns were recorded on a Bruker D8 diffractometer with high-intensity Cu Kα radiation (Bruker Co., Germany). Raman spectra were recorded on a RM 2000 microscopic confocal Raman spectrometer (Renishaw, UK). X-ray

photoelectron spectrometry (XPS) analyses were measured by a VG MultiLab 2000 system with a monochromatic Mg-K a source operated at 20 kV. UV-vis diffuse reflectance spectra (UV-vis DRS) were measured by UV-2450 spectrophotometer (Shimadzu, Japan) with $BaSO_4$ as reflectance sample. The PEC measurements and all the electrochemical were performed by using CHI 660B electrochemical workstation (Shanghai Chenhua Instrument Co. Ltd., China) with a standard three-electrode cell system with the ITO as a working electrode, a platinum (Pt) wire as a counter electrode, and a saturated calomel electrode (SCE) as a reference electrode. All the PEC measurements were performed in 0.1 mol L^{-1} PBS at 0 V and a 250 W Xe lamp (CHF-XM35-500W, Beijing Chang tuo) was utilized as the irradiation source (passing through a 400 nm UV-cut filter). Current-time (I–t) method was used for the whole PEC experiments. Electrochemical impedance spectroscopy (EIS) was performed in the 0.1 mol L^{-1} KCl solution containing 5 mmol L^{-1} $[Fe(CN)_6]^{3-/4-}$ with a frequency from 0.01 Hz to 10 kHz at a constant potential of 0.23 V.

2.3 Preparation of $BiPO_4$/3DNGH

$BiPO_4$/3DNGH nanocomposites were synthesized by a one-pot hydrothermal route. In a typical synthesis, a certain amount of GO powder was dispersed in 10 mL water with sonication to obtain a homogeneous suspension. Then, 0.5 mmol $Bi(NO_3)_3 \cdot 5H_2O$, 0.5 mmol $NaH_2PO_4 \cdot 2H_2O$, 1.3 mmol glycine were sequentially added into the previous prepared suspension. After stirring for 1 h, the as-obtained brown suspension was transferred into a Teflon-lined autoclave, and then kept at 180 °C for 12 h. Finally, the synthesized hydrogels were washed with distilled water for several times and the wet hydrogel was freeze-dried to obtain the $BiPO_4$/3DNGH nanocomposites. The $BiPO_4$/3DNGH nanocomposites with different ratios of GO to

$BiPO_4$ (2, 3, 5, 6, 7 and 10 wt%) were prepared using the same process. For comparison, following the same procedure above, the pristine $BiPO_4$ were prepared without adding GO and glycine, and 3DNGH were prepared without adding $Bi(NO_3)_3 \cdot 5H_2O$ and $NaH_2PO_4 \cdot 2H_2O$. In addition, the $BiPO_4$/rGO and $BiPO_4$/NG nanocomposites were prepared according to the previous literature (Chen et al. 2017b; Qian et al. 2015).

2.4 Fabrication of the modified electrodes

Prior to modification of ITO, the ITO electrodes were treated by NaOH (1 mol L^{-1}) solution and then were ultrasonically rinsed several times in distilled water and alcohol to remove any residue. For preparation of the modified electrode, 5 mg mL^{-1} $BiPO_4$/3DNGH suspension was prepared by dispersing 5 mg of $BiPO_4$/3DNGH in 1 mL DMF with ultrasonic agitation. Forty microliters of $BiPO_4$/3DNGH suspension (5 mg mL^{-1}) was dropped onto the surface of ITO with a fixed area of 0.5 cm^2 and then dried in ambient air to obtain $BiPO_4$/3DNGH modified ITO electrode (denoted as $BiPO_4$/3DNGH/ITO). For comparison, $BiPO_4$ $BiPO_4$/rGO and $BiPO_4$/NG modified ITO electrodes were prepared with the same procedure above.

2.5 Fabrication of the photoelectrochemical aptasensor

To construct the Tc aptasensor, twenty microliters of 2.5 μmol L^{-1} Tc aptamer solution was coated onto the $BiPO_4$/3DNGH/ITO. The obtained aptamer/$BiPO_4$/3DNGH/ITO were dried in ambient air and rinsed with 0.1 mol L^{-1} PBS to remove any unbounded aptamers. Twenty microliters Tc solutions with a variety of concentrations were incubated on the as-prepared

aptamer/$BiPO_4$/3DNGH/ITO electrode at room temperature and then the electrodes were rinsed thoroughly with 0.1 mol L^{-1} PBS followed by the respective PEC measurements.

3. Results and discussion

3.1 Characterization of the samples

The morphology of the as-prepared pristine $BiPO_4$, 3DNGH and $BiPO_4$/3DNGH were characterized by SEM and TEM. As shown in Fig. S1A, $BiPO_4$ nanorods formed at the length of 500-800 nm. Fig. S1B displays the typical continuous fold framework of 3DNGH with porous structure. When 3DNGH and $BiPO_4$ form nanocomposites, $BiPO_4$/3DNGH nanocomposites exhibited a well cross-linked porous structure and the $BiPO_4$ nanorods were anchored onto the 3DNGH surface (Fig. 1A). The TEM image of $BiPO_4$/3DNGH can more clearly reveal that $BiPO_4$ nanorods were randomly distributed on the 3DNGH surface (Fig. S1C). Meanwhile, the photograph of $BiPO_4$/3DNGH before and after freeze-dried displayed in Fig. S1D showed the obvious hydrogel appearance of the as-prepared $BiPO_4$/3DNGH.

Fig. 1B shows the XRD pattern of as-prepared 3DNGH, pristine $BiPO_4$, and $BiPO_4$/3DNGH, respectively. The pristine $BiPO_4$ (curve a) displayed the diffraction peaks at 2θ = 19.1º, 21.4º, 25.3º, 27.1º,29.1º, 31.2º, 34.5º, 36.8º, 38.6º, 41.4º, 42.8º, 46.3º, 52.1º and 58.8º, which might be assigned to the (011), (–111), (111), (200), (120), (012), (–202), (112), (022), (130), (–131), (212), (–322) and (040) planes, respectively. All the diffraction peaks of the as-synthesized $BiPO_4$ nanorods could be indexed to the diffraction of the monoclinic phase $BiPO_4$ (JCPDA No.15-0767) (Chen

et al. 2017b; Liu et al. 2015c). The XRD pattern of $BiPO_4$/3DNGH nanocomposites (curve c) was almost no difference with the pristine $BiPO_4$, and the characteristic peaks of 3DNGH (curve b) at around 26º was not detected demonstrating that the 3DNGH did not stack on each other and disperse on the surface of $BiPO_4$ nanorods homogeneously (Zhang et al. 2014).

Raman spectra of the as-prepared samples are presented in Fig. 1C. For pristine $BiPO_4$ (curve a), the typical vibrational bands between 50 and 300 cm^{-1} were attributed to the vibration of Bi–O bonds (Gao and Wang 2013). The bands between 350 and 700 cm^{-1} were attributed to the bending vibration modes of the PO_4 units. The Raman spectra presented bands at 970 and 1041 cm^{-1} might be assigned to the symmetric and asymmetric stretching modes of the PO_4 units, respectively (Zhu et al. 2016). The Raman spectrum of 3DNGH contains two prominent peaks at 1348 and 1590 cm^{-1}, corresponding to the D and G bands, respectively. The D band was assigned to the structural defects and staging disorder. The G band corresponded to the zone center E_{2g} mode of the sp^2 carbon domains. It is widely recognized that the intensity ratio of D and G band (I_D/I_G) is used to measure the degree of defects in the graphene-based material (Jiang et al. 2015). The $BiPO_4$/3DNGH revealed higher intensity ratio of I_D/I_G (1.16) than 3DNGH (1.05), which indicated that there were defects in the nanocomposites. The photoelectrochemical properties of nanocomposites may be improved by the defects of 3DNGH (Zhang et al. 2012).

As shown in Fig. S3A, the survey XPS spectra indicated that the $BiPO_4$/3DNGH nanocomposites were composed of elements of Bi, P, O, C and N. The high-resolution N 1s spectrum of $BiPO_4$/3DNGH was presented in Fig. S3B, indicating the presence of two forms nitrogen, namely, pyridinic N (401.1 eV) and pyridinic N (402.3 eV) (Hao et al. 2017). The pyridinic nitrogen in the $BiPO_4$/3DNGH can provide a pair of

electrons for conjugation with π-conjugated rings, which can introduce electron donor properties to 3DNGH and improve the electrochemical performance of nanocomposites (Jiang et al. 2016a). The pyrrolic nitrogen has higher charge mobility in 3DNGH due to its better electron-donor characteristics. (Yang et al. 2013). Meanwhile, elemental mapping images (EMIs) revealed the existence of C, N, O, P and Bi elements (Fig. S2). The results above clearly confirmed the successful preparation of the $BiPO_4$/3DNGH nanocomposites

In addition, the band gap energy (E_g) of semiconductor material could be estimated by Kubelka-Munk transformation: $\alpha h\upsilon = A(h\upsilon - E_g)^{n/2}$ in which α, υ, E_g and A are the absorption coefficient, light frequency, bandgap energy and a constant for the material. Moreover, n was 2 for a direct transition or 4 for an indirect transition, respectively (Jiang et al. 2016a). Fig. 1D displays the bandgap of pristine $BiPO_4$ and $BiPO_4$/3DNGH based on the $(\alpha h\upsilon)^{1/2}$ versus ($h\upsilon$) plot. As can be seen, the bandgap of pristine $BiPO_4$ (curve a) was estimated to be 3.85 eV, which was in good agreement with the values reported in previous literature (Tan et al. 2017). The bandgap of $BiPO_4$/3DNGH was 2.10 eV (curve c), which was greatly narrower than that of pristine $BiPO_4$. This result might be attributed to the presence of 3DNGH with no band gap (curve b), making 3DNGH a highly absorptive material (Liu et al. 2015a). The results above indicated that the $BiPO_4$/3DNGH nanocomposites would exhibit more excellent PEC properties under the visible light irradiation.

3.2 PEC response of the modified electrode

Fig. 2A presents the photocurrent responses of different modified electrodes in 0.1 mol L^{-1} PBS under visible light irradiation. The photocurrent of pristine $BiPO_4$/ITO and 3DNGH/ITO could be negligible (curve a and curve b). When

3DNGH was introduced into the nanocomposites, the photocurrent intensity of the $BiPO_4$/3DNGH/ITO was remarkably enhanced to 3.05 μA (curve e). It could be explained that 3DNGH could enhance charge transfer rate to promote efficient electron-hole separation and suppress the rapid recombination of electrons and holes, resulting the enhanced photocurrent intensity (Mou et al. 2014; Wang et al. 2014b). Furthermore, compared to $BiPO_4$/rGO/ITO and $BiPO_4$/2DNG/ITO, the photocurrent intensity of the $BiPO_4$/3DNGH/ITO was 4.1-fold and 2.3-fold enhancement respectively, the photocurrent signal of $BiPO_4$/3DNGH/ITO was the highest. The reason might be attributed that the porous structure of three-dimensional graphene could be beneficial for the anchoring of $BiPO_4$ nanorods and the introduction of nitrogen atoms is an effective way to improve the conductivity of graphene and suppress the electrons and holes recombination (Hao et al. 2017; Jiang et al. 2016b), resulting the enhanced photocurrent intensity. To further verify the supposition above, EIS analysis was investigated. As can be seen in Fig. 2B, it can be found that the electron-transfer resistance (R_{et}) value of 3DNGH/ITO, the pristine $BiPO_4$/ITO and $BiPO_4$/3DNGH/ITO was about 36, 112 and 57 Ω, respectively, implying 3DNGH could effectively enhance electron transport ability of the pristine $BiPO_4$. The R_{et} of $BiPO_4$/3DNGH/ITO was the smallest compared to $BiPO_4$/ITO, $BiPO_4$/rGO/ITO and $BiPO_4$/2DNG/ITO, indicating that 3DNGH can accelerate electron transfer to cause R_{et} value to decrease (Wang et al. 2014b).

3.3 Fabrication of the PEC aptasensing platform

Fig. 3A presents the PEC behaviors of different modified electrodes. As can be seen from Fig. 3A, $BiPO_4$/3DNGH nanocomposites (curve a) exhibited an excellent PEC performance and displayed a photocurrent of 3.05 μA. When the aptamer was

modified on the $BiPO_4$/3DNGH/ITO electrode (curve b), the photocurrent intensity remarkably decreased, which resulting a low PEC background signal for the further detection of Tc. When the Tc molecules were introduced, the photocurrent response significantly increased (curve c), which might be attributed to the reason that the aptasensor specifically captures the Tc, Tc-aptamer comlplex formed and the aptamer released from the sensing interface.

EIS has been widely applied in the study of interfacial charge transfer processes (Wang et al. 2014a). Fig. 3B shows the impedance spectra of the different modified electrodes associated with the aptasensor. When aptamers were modified on $BiPO_4$/3DNGH/ITO electrode, the R_{et} remarkably increased from 56.8 to 135.8 Ω, which indicated that aptamers were successfully assembled on the $BiPO_4$/3DNGH surface via the π−π stacking interaction between 3DNGH and aptamer. When Tc molecules were introduced, the aptasensor could specifically react with the Tc, the impedance of Tc/aptamer-$BiPO_4$/3DNGH/ITO (curve c) became smaller than aptamer-$BiPO_4$/3DNGH /ITO (curve b). The reason might be attributed to the Tc could interact with the aptamer to form a Tc-aptamer complex, which break up π−π stacking interaction, leading to the good separation between Tc-aptamer complex and $BiPO_4$/3DNGH in solution (Meng et al. 2016). All these results indicated that the proposed PEC aptasensor was successful fabricated and could be applied to the detection of Tc.

Scheme 1 displays the procedure and the mechanism of the constructed PEC aptasensor for the selective detection of Tc. Owing to the introduction of 3DNGH which improving the charge transfer, the photocurrent intensity of $BiPO_4$/3DNGH nanocomposites exhibited a powerful visible light photoelectrochemical response. When the aptamers were introduced , owing to the presence of aptamer molecules

which enhanced the steric hindrance of the electrode interface and block the electron transfer, the photoelectrochemical response drastically decreased (Yan et al. 2015). Then in the presence of Tc molecules, the aptamer modified on $BiPO_4$/3DNGH electrode could specifically and sensitively capture Tc molecules on the surface of aptasensor, followed Tc-aptamer complex formed and the aptamer released from the sensing interface (Meng et al. 2016), the photocurrent of the aptasensor was markedly enhanced. Therefore, the quantitative analysis of Tc can be achieved by monitoring the photocurrent of aptasensor.

3.4 Optimization of conditions for PEC aptasensor

For the proposed PEC aptasensor, some important parameters affecting photocurrent intensity should be optimized. As all known in a PEC sensor, the content of different components in nanocomposites has a great influence on the intensity of photocurrent. Fig. S4A displays the PEC behavior of different GO contents in $BiPO_4$/3DNGH nanocomposites. It could be seen clearly that the photocurrent of $BiPO_4$/3DNGH/ITO electrode increased gradually with the weight ration of GO increasing from 2% to 5% wt. This phenomenon might be due to the fact that 3DNGH can inhibit the recombination of photogenerated electrons and holes and thus improve the electron-hole pair charge separation efficiency, which resulted in the enhanced photocurrent signal. However, the photocurrent response was gradually decreased when the weight ratio of GO exceeded 5% wt. The result might be due to the light "shielding effect" of graphene where the excessive amounts of graphene lead to the active sites of the $BiPO_4$ are hindered as well as reducing the efficiency of light passing through the active materials $BiPO_4$/3DNGH (Okoth et al. 2016). Therefore, $BiPO_4$/3DNGH$_{5\%}$ was selected as the optimal photoactive material in this work.

The concentration of the aptamer had an important influence on the performance of the constructed aptasensor. As displayed in Fig. S4B, the intensity of the photocurrent gradually declined with increasing the aptamer concentration up to 2.5 μmol L^{-1}. However, when the concentration of the aptamer exceeds 2.5 μmol L^{-1}, the intensity of the photocurrent nearly reached a plateau. Therefore, 2.5 μmol L^{-1} was selected as the optimum aptamer concentration and used in the following experiment.

3.5 Sensitive and selective PEC aptasensor of Tc

The fabricated label-free aptasensor was applied to the PEC determination of Tc under optimized conditions. Fig. 4A exhibits the PEC responses of the aptamer-$BiPO_4$/3DNGH/ITO electrodes to Tc at different concentrations under visible light illumination. The photocurrent response gradually increased with increasing concentrations of Tc, which was attributed to releasing more Tc-aptamer complex. A good linear relationship was obtained between the photocurrent intensity of aptasensor and the logarithm of Tc concentrations in range of 0.1 nmol L^{-1} to 1 μmol L^{-1} (R^2 = 0.991) (Fig. 4B). Moreover, the detection limit was estimated to be 0.033 nmol L^{-1} (defined as S/N = 3), which was a lower detection limit compared with many previously published reports for the detection of Tc (Table S1)

To investigate the selectivity of the proposed PEC sensor, the influence of other antibiotics including chloramphenicol (CAP), kanamycin (KAN), ciprofloxacin(CIP), oxytetracycline (OTC) as interfering substances on the photocurrent intensity were investigated. As can be seen in Fig. 4C, 100 nmol L^{-1} of the other antibiotics did not display obvious photocurrent change on the aptamer-$BiPO_4$/3DNGH/ITO electrode compared to Tc, which exhibited that the proposed PEC sensor showed excellent selectivity for Tc detection.

The photocurrent response was recorded under nine on/off irradiation cycles in Fig. 4D and no noticeable variation occurred indicated that the photocurrent signals were quite stability under visible light illumination. Meanwhile, the PEC aptasensor retained 96.3% of its photocurrent response after storage under 4 °C for 3 weeks, indicating the PEC sensor has the good long-term stability. Moreover, compared to a number of freshly prepared aptamer-$BiPO_4$/3DNGH/ITO electrodes, a relative standard deviation (RSD) was recorded as 5.3%, indicating that the proposed sensor has good reproducibility.

3.6 Real sample analysis

To evaluate the feasibility of the proposed PEC aptasensor in real samples, the milk samples from a local supermarket (Zhenjiang, PR China) was chosen as the real sample. The standard addition method was adopted and different concentrations of Tc were added into the real sample. The prepared real sample was analyzed with the prepared sensor and the intensity of photocurrent was recorded. Table 1 lists the recovery in the range of 98.0 ~ 105.3% with the RSD of 2.3 ~ 3.8%. These results indicated the fabricated PEC aptasensor was feasible and could be applied for analysis of real samples.

4. Conclusions

In summary, we prepared $BiPO_4$/3DNGH nanocomposites to serve as visible light-responsive material by a facile one-pot hydrothermal route. The porous structure of 3DNGH significantly promoted the separation efficiency and transfer rate of the photoinduced electron-hole pairs and enhanced visible light absorption of $BiPO_4$. The $BiPO_4$/3DNGH nanocomposites displayed excellent PEC performances comparing to

the pristine $BiPO_4$, $BiPO_4$/rGO and $BiPO_4$/NG. Using $BiPO_4$/3DNGH as a visible light-responsive material and aptamer as a biorecognition element, a label-free PEC aptasensor for high sensitive and selective detection of Tc was successfully constructed. Moreover, the proposed PEC aptasensor also successfully applied for analysis of real samples, indicating the fabricated PEC aptasensor based on visible light-responsive $BiPO_4$/3DNGH could provide a new platform for specific detection in biomedical, food and environment analysis.

Acknowledgements

The present work was financial supported by the National Natural Science Foundation of China (Nos. 21375050, 21675066 and 61601204), Provincial Natural Science Foundation of Jiangsu (No. BK20160542), China Postdoctoral Science Foundation (No. 2017T100330), the Research Foundation of Zhenjiang Science and Technology Bureau (No. NY2016011), and the Foundation of Key Laboratory of Sensor Analysis of Tumor Marker, Ministry of Education, Qingdao University of Science and Technology (No. SATM201807).

References

Bousova, K., Senyuva, H., Mittendorf, K., 2013. J. Chromatogr. A 1274, 19-27.

Chen, W.F., Li, S.R., Chen, C.H., Yan, L.F., 2011. Adv. Mater. 23, 5679-5683.

Chen, S.B., Nan, H., Zhang, X., Yan, Y.T., Zhou, Z., Zhang, Y., Wang, K., 2017. J. Mater. Chem. B 5, 3718-3727.

Chen, Z.G., Chen, X.L., Di, J., Liu, Y.L., Yin, S., Xia, J.X., Li, H.M., 2017. J. Colloid. Interface Sci. 492, 51-60.

Choi, B.G., Yang, M.H., Hong, W.H., Choi, J.W., Huh, Y.S., 2012. ACS Nano 6,

4020-4028.

Dong, X.C., Wang, X.W., Wang, L.H., Song, H., Zhang, H., Huang, W., Chen, P., 2012. ACS Appl. Mater. Interfaces 4, 3129-3133.

Gan, T., Shi, Z.X., Sun, J.Y., Liu, Y.M., 2014. Talanta 121, 187-193.

Gao, E., Wang, W., 2013. Nanoscale 5, 11248-11256.

GB 21317—2007. National Standard of the People's Republic of China.

Hao, N., Zhang, X., Zhou, Z., Hua, R., Zhang, Y., Liu, Q., Qian, J., Li, H.N., Wang, K., 2017. Biosens. Bioelectron. 97, 377-383.

Hou, J., Zhang, H.C., Yang, Q., Li, M.Z., Jiang, L., Song, Y.L., 2015. Small 11, 2738-2742.

Ibarra, I.S., Rodriguez, J. A., Miranda, J. M., Vega, M., Barrado, E., 2011. J. Chromatogr. A 1218, 2196-2202.

Jiang, D., Du, X.J., Chen, D.Y., Li, Y.Q., Hao, N., Qian, J., Zhong, H., You, T.Y., Wang, K., 2016a. Carbon 102, 10-17

Jiang, D., Du, X.J., Chen, D.Y., Zhou, L., Chen, W., Li, Y.Q., Hao, N., Qian, J., Liu, Q., Wang, K., 2016. Biosens. Bioelectron. 83, 149-155.

Jiang, D., Du, X.J., Liu, Q., Zhou, L., Qian, J., Wang, K., 2015. ACS Appl. Mater. Interfaces 7, 3093-3100.

Lau, C.W., Lu, J.Z., Kai, M., 2004. Anal. Chim. Acta 503, 235-239.

Li, L., Zhang, Y., Zhang, L.N., Ge, S.G., Liu, H.Y., Ren, N., Yan, M., Yu, J.H., 2016. Anal. Chem. 88, 5369-5377.

Liu, K., Zhu, Z.H., Li, X.J., Zhang, J.F., Yuan, X.D., Guo, C.C., Xu, W., Qin, S.Q., 2015a. ACS Photonics 2, 797-804.

Liu, Y., Yan, K., Okoth, O.K., Zhang, J.D., 2015. Biosens. Bioelectron. 74, 1016-1021.

Liu, Y., Yan, K., Zhang, J.D., 2016. ACS Appl. Mater. Interfaces 8, 28255-28264.

Liu, Y., Yang, H.L., Yang, S., Hu, Q.W., Cheng, H.B., Liu, H.Y., Qiu, Y.S., 2013. J. Chromatogr. B 917-918, 11-17.

Liu, Y.F., Yao, W.Q., Liu, D., Zong, R.L., Zhang, M., Ma, X.G., Zhu, Y.F., 2015. Appl. Catal. B: Environ. 163, 547-553.

Lu, M.N., Yuan, G.T., Wang, Z.S., Wang, Y.Y., Guo, J., 2015. Nanoscale Res Lett 10, 385.

Meng, H.M., Liu, H., Kuai, H.L., Peng, R.Z., Mo, L.T., Zhang, X.B., 2016. Chem. Soc. Rev. 45, 2583-2602.

Mo, Z.Y., Zheng, R.P., Peng, H.L., Liang, H.G., Liao, S.J., 2014. J. Power. Sources .245, 801-807.

Mou, Z.G., Wu, Y.J., Sun, J.H., Yang, P., Du, Y.K., Lu, C., 2014. ACS Appl. Mater. Interfaces 6, 13798-13806.

Okoth, O.K., Yan, K., Liu, Y., Zhang, J.D., 2016. Biosens. Bioelectron. 86, 636-642.

Pan, C., Zhu, Y.F., 2010. Environ. Sci. Technol. 44, 5570-5574.

Qian, J., Yang, Z.T., Wang, C.Q., Wang, K., Liu, Q., Jiang, D., Yan, Y.T., Wang, K., 2015. J. Mater. Chem. A 3, 13671-13678.

Ramezani, M., Mohammad Danesh, N., Lavaee, P., Abnous, K., Mohammad Taghdisi, S., 2015. Biosens. Bioelectron. 70, 181-187.

Shen, L., Chen, J., Li, N., He, P.L., Li, Z., 2014. Anal. Chim. Acta 839, 83-90.

Tan, G.Q., She, L.N., Liu, T., Xu, C., Ren, H.J., Xia, A., 2017. Appl. Catal. B: Environ. 207, 120-133.

Tan, H.L., Ma, C.J., Song, Y.H., Xu, F.G., Chen, S.H., Wang, L., 2013. Biosens. Bioelectron. 50, 447-452.

Wang, H.B., Maiyalagan, T., Wang, X., 2012. ACS Catal. 2, 781-794.

Wang, K.W., Zhang, R.H., Sun, N., Li, X.P., Wang, J., Cao, Y., Pei, R.J., 2016. ACS Appl Mater Interfaces 8, 25834-25839.

Wang, L.N., Ma, W.G., Gan, S.Y., Han, D.X., Zhang, Q.X., Niu, L., 2014a. Anal. Chem. 86, 10171-10178.

Wang, S.L., Li, J.J., Zhou, X.D., Zheng, C.C., Ning, J.Q., Zhong, Y.J., Hu, Y., 2014b. J Mater Chem. A 2, 19815-19821

Xi, F.N., Zhao, D.J., Wang, X.W., Chen, P., 2013. Electochem. Commun. 26, 81-84.

Xu, J.J., An, M.G., Yang, R., Tan, Z.J., Hao, J., Cao, J., Peng, L.Q., Cao, W., 2016. J.Agric. Food Chem. 64, 2647-2654.

Yan, K., Liu, Y., Yang, Y.H., Zhang, J.D., 2015. Anal. Chem. 87, 12215-12220.

Yang, S.H., Song, X.F., Zhang, P., Gao, L., 2013. ACS Appl. Mater. Interfaces 5, 3317-3322

Ye, H.F., Lin, H.L., Cao, J., Chen, S.F., Chen, Y., 2015. J Mol Catal A-Chem 397, 85-92.

Zang, Y., Lei, J.P., Ju, H.X., 2017. Biosens. Bioelectron. 96, 8-16.

Zhang, K.J., Han, P.X., Gu, L., Zhang, L.X., Liu, Z.H., Kong, Q.S., Zhang, C.J., Dong, S.M., Zhang, Z.Y., Yao, J.H., Xu, H.X., Cui, G.L., Chen, L.Q., 2012. ACS Appl. Mater. Interfaces 4, 658-664.

Zhang, X.J., Wang, G.S., Cao, W.Q., Wei, Y.Z., Liang, J.F., Guo, L., Cao, M.S., 2014. ACS Appl. Mater. Interfaces 6, 7471-7478.

Zhu, Y.Y., Ling, Q., Liu, Y.F., Wang, H., Zhu, Y.F., 2016. Appl. Catal. B: Environ. 187, 204-211.

Zhuang, J.Y., Lai, W.Q., Xu, M.D., Zhou, Q., Tang, D.P., 2015. ACS Appl. Mater. Interfaces 7, 8330-8338.

Figure captions

Scheme 1 Schematic illustration of PEC aptasensor for detecting Tc based on $BiPO_4$/3DNGH nanocomposites.

Fig. 1 (A) The SEM image of $BiPO_4$/3DNGH, (B) XRD pattern, (C) Raman spectra and (D) Plot of $(Ah\upsilon)^2$ versus the energy ($h\upsilon$) for the band gap energy of pristine $BiPO_4$ (a), 3DNGH (b) and $BiPO_4$/3DNGH (c).

Fig. 2 (A) Photocurrent responses and (B) EIS spectra of pristine $BiPO_4$/ITO (a), 3DNGH/ITO (b), $BiPO_4$/rGO/ITO (c), $BiPO_4$/2DNG/ITO (d) and $BiPO_4$/3DNGH/ITO (e).

Fig. 3 (A) Photocurrent responses and (B) EIS spectra of $BiPO_4$/3DNGH/ITO (a), aptamer-$BiPO_4$/3DNGH/ITO (b) and Tc/aptamer-$BiPO_4$/3DNGH/ITO (c).

Fig. 4 (A) Photocurrent responses of the aptamer-$BiPO_4$/3DNGH/ITO at different concentrations of Tc: (a→j: $0.01 \rightarrow 10^4$ nmol L^{-1}), (B) The corresponding linear calibration curve for Tc detection, (C) PEC responses of aptamer-$BiPO_4$/3DNGH/ITO toward various antibiotics at 100 nmol L^{-1} and (D) Stability test of the resulting aptasensor under nine on/off cycles.

Table 1 Analytical results of Tc in milk samples using the proposed method (n = 3)

Scheme 1

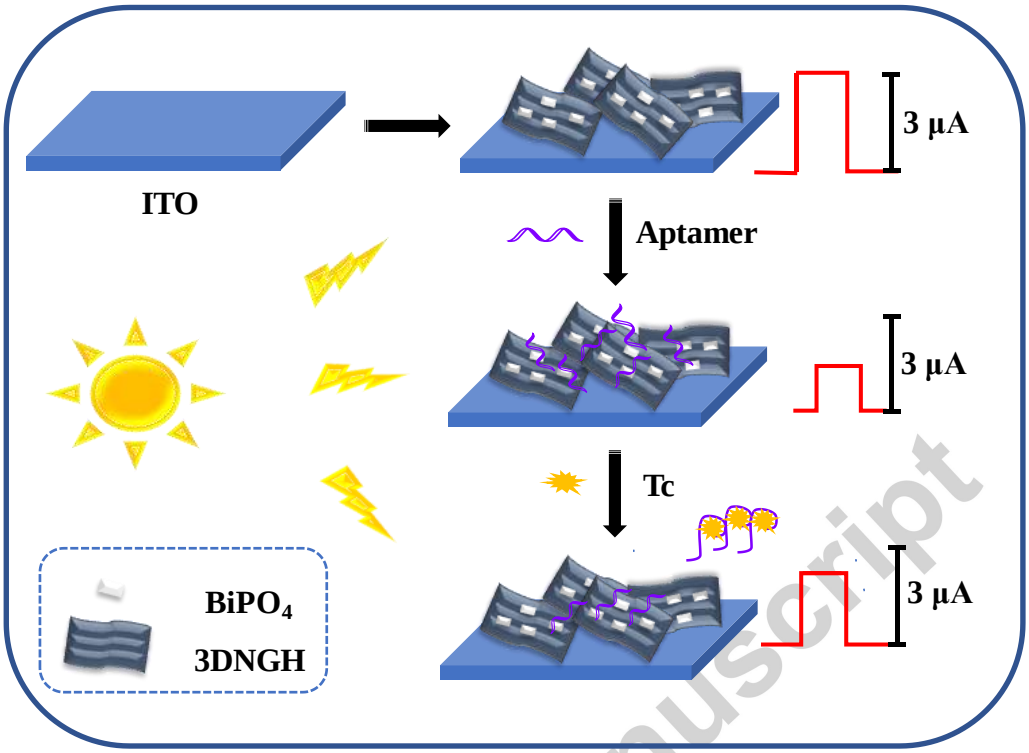

Fig. 1

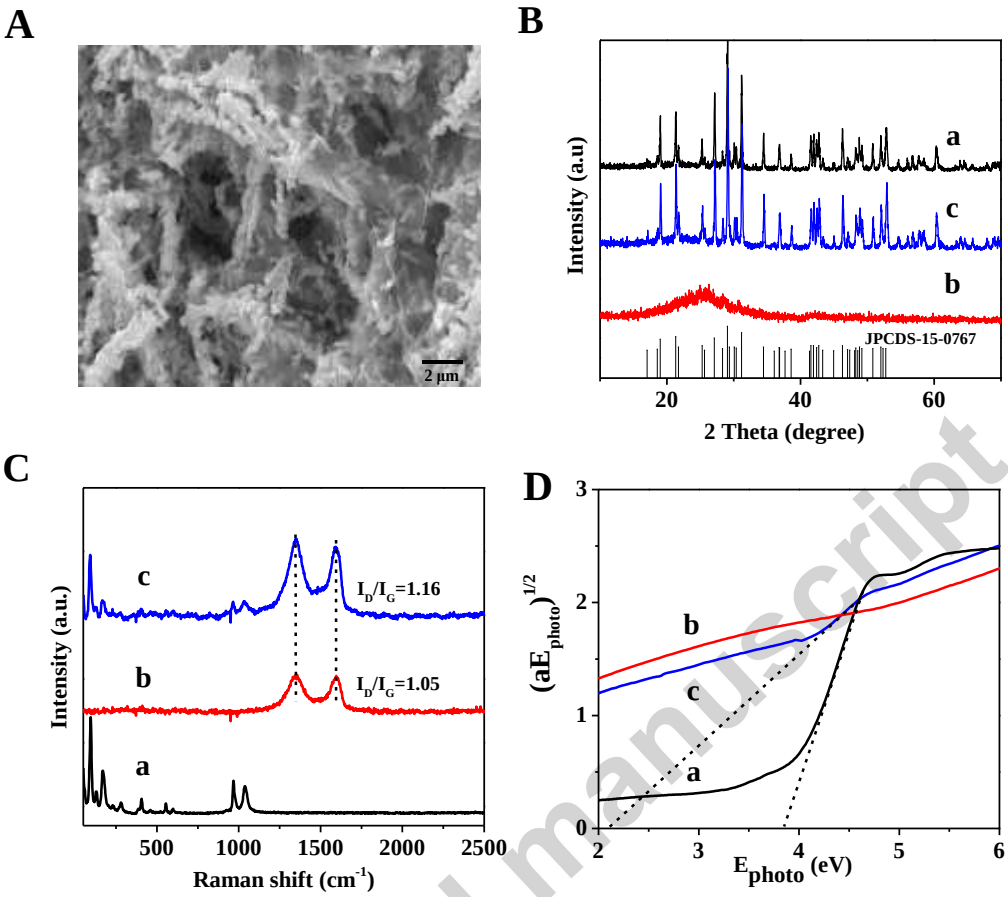

Fig. 2

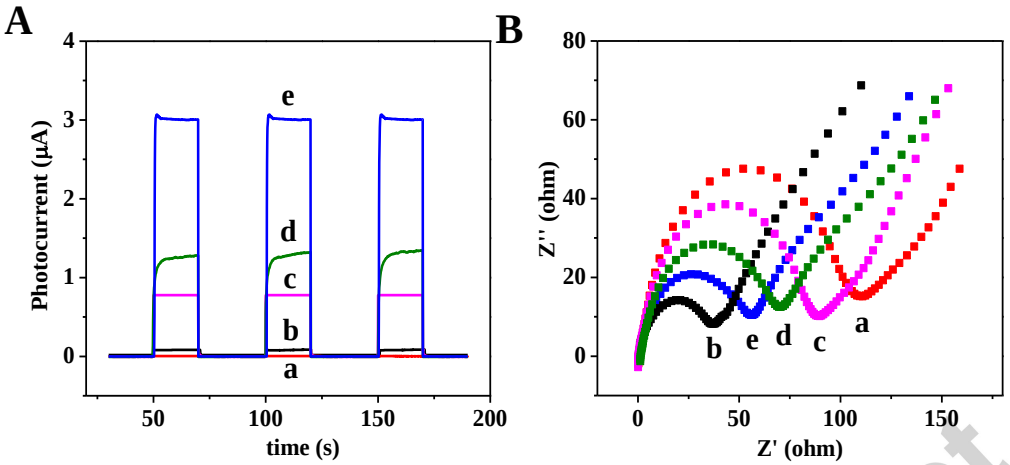

Fig. 3

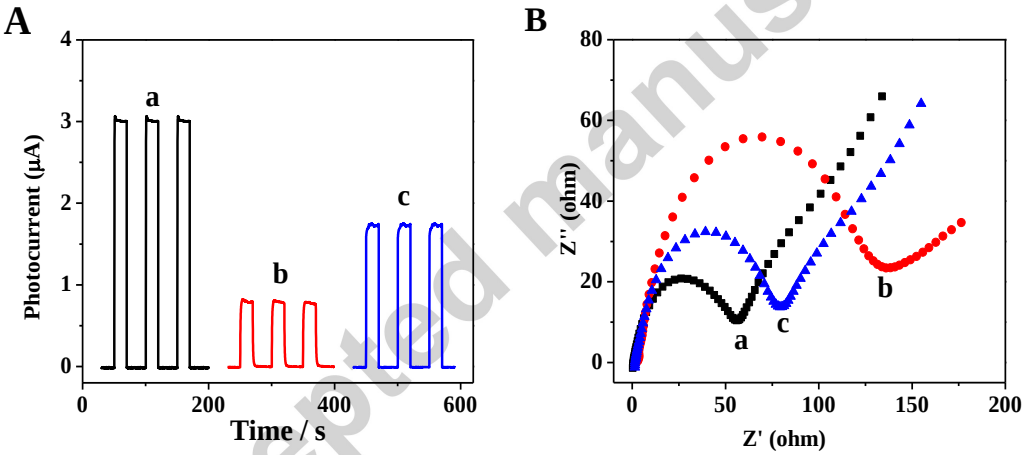

Fig. 4

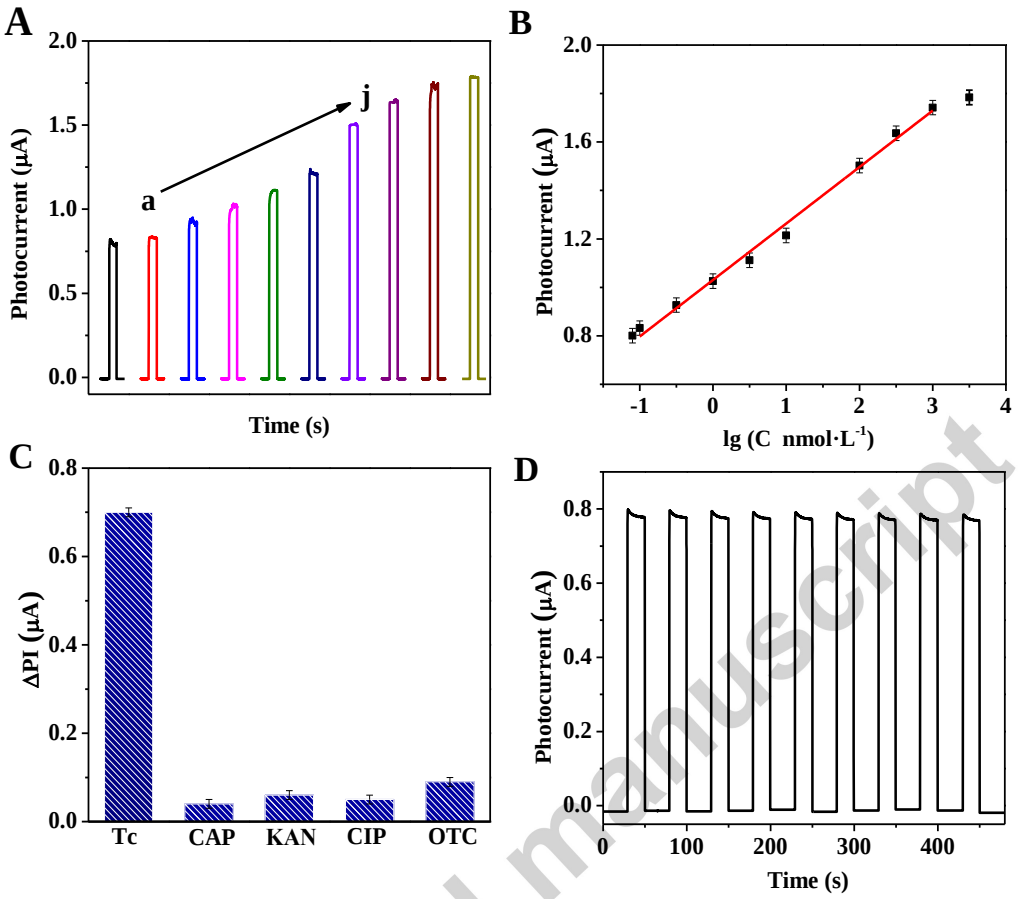

Table 1 Analytical results of Tc in milk samples using the proposed method (n = 3)

	Spiked (nmol L^{-1})	Found (nmol L^{-1}) (mean [a] ± SD [b])	Recovery (%)	RSD (%)
Sample 1	0	0	—	—
Sample 2	10.0	9.8 ± 0.3	98.0	2.6
Sample 3	100.0	105.3 ± 4.0	105.3	3.8
Sample 4	200.0	204.2 ± 4.7	102.1	2.3

[a] mean, average value of three tests.

[b] SD, standard deviation.

Highlights

- $BiPO_4$/3DNGH with super visible light-responsive was prepared for the first time.
- The photocurrent of $BiPO_4$/3DNGH was greatly enhanced compared with pristine $BiPO_4$, $BiPO_4$/rGO and $BiPO_4$/NG
- A visible light-driven PEC tetracycline aptasensor was successfully established.
- The proposed aptasensor exhibited excellent selectivity and sensitivity for tetracycline detection.